6-15-1998

Upper Ocean Heat and Freshwater Advection in the Western Pacific Ocean

Michele Y. Morris
University of California

Dean H. Roemmich
University of California

Gary Meyers
CSIRO

Robert H. Weisberg
University of South Florida, weisberg@marine.usf.edu

JOURNAL OF GEOPHYSICAL RESEARCH, VOL. 103, NO. C6, PAGES 13,023–13,039, JUNE 15, 1998

Upper ocean heat and freshwater advection in the western Pacific Ocean

Michele Y. Morris[1] and Dean H. Roemmich
Scripps Institution of Oceanography, University of California, San Diego, La Jolla

Gary Meyers
Marine Laboratory, Division of Oceanography, CSIRO, Hobart, Tasmania, Australia

Robert Weisberg
University of South Florida, Saint Petersburg

Abstract. Mean net surface heating of the Pacific Ocean shows areas of high heat gain in the eastern tropics and heat loss in the western midlatitudes. For steady state conditions, westward and poleward transport of heat is implied. Mean geostrophic and Ekman fluxes of heat and freshwater through the sides of a western tropical Pacific box bounded by World Ocean Circulation Experiment (WOCE) high-resolution expendable bathythermograph (XBT) transects are presented. Water mass properties of currents transporting heat and freshwater through the enclosed region are seen to be modified in transit. Net transport convergences within the volume of water extending to 800 m in the vertical show a shallow ocean circulation cell ($\sigma_\theta < 26$) with relatively dense subtropical gyre water entering the volume and lighter water leaving in western boundary currents, eastward flowing tropical currents, Ekman flow, and outflow to the Indian ocean. Surface buoyancy fluxes are dominated by freshwater rather than heat fluxes. Freshwater gain through the surface allows warm, salty water to enter in the same density range as cool, fresh water leaving the volume. For steady state conditions the XBT-derived oceanic heat convergence of 0 ± 0.3 PW implies negligible heat loss to the atmosphere. Traditional surface heat flux climatologies predict too much heat gain. Part of the discrepancy may be due to anomolous meteorological conditions during the XBT experiment (1987–1995). Oceanic freshwater divergence of 0.70 ± 0.08 Sv falls in the range of climatological predictions from surface freshwater gain.

1. Introduction

An estimate of mean net surface heating of the Pacific Ocean from *da Silva et al.* [1995] is shown in Figure 1a. Regions of high heat gain can be seen in the eastern tropical Pacific. This area overlies cool sea surface temperatures resulting from upwelled water along the equator. Heat is lost to the atmosphere in midlatitudes where warm boundary current water flows poleward and is strongly cooled by dry continental air. For oceanic steady state conditions, advection of heat from the eastern tropics to the western midlatitudes is implied. Previous studies have focused on the meridional transport of heat required to equilibrate excess heat gained at the tropics with that lost at high latitudes [e.g., *Talley*, 1984; *Roemmich and McCallister*, 1989]. The focus of this study is on the zonal and meridional redistribution of heat implied by zonally asymmetric surface heating of the tropical and subtropical Pacific.

Long time series of high-resolution (HR) expendable bathythermograph (XBT) measurements provide high-quality estimates of heat advection in the upper ocean, which can be used to determine oceanic pathways of heat transfer. Mean observations from four HR XBT sections bounding a west central Pacific volume (see Figure 1 for ship tracks) are used in this study. Oceanic conditions around the edges of the boxed volume are varied, ranging from subtropical gyre flow through the northern and southern parts of the volume to swift tropical currents close to the equator. The respective importance of these currents to the mean heat and freshwater balances of the tropical/subtropical Pacific will be investigated.

A climatological estimate of net freshwater flux out of the ocean from *da Silva et al.* [1995] is shown in Figure 1b, and it can be seen that freshwater is gained by the ocean across a large fraction of the area bounded by the HR XBT transects. Precipitation exceeds evaporation in the warm pool and under the South Pacific and Intertropical Convergence Zones. It is clear from Figures 1a and 1b that the surface waters will be modified as they flow through the enclosed region. The HR XBT observations allow the water mass transformation rates within the volume to be quantified.

The HR XBT temperature measurements extend to 800 m, which is relatively shallow compared with the ocean depth. This may seem a serious limitation at first; however, it should be noted that a high fraction of the stratification occurs in the upper kilometer for the tropical and subtropical oceans. The exception is the equatorial zone where currents remain strong throughout the water column. The unmeasured deep flow field

[1]Now at Woods Hole Oceanographic Institution, Woods Hole, Massachusetts.

Paper number 98JC00195.
0148-0227/98/98JC-00195$09.00

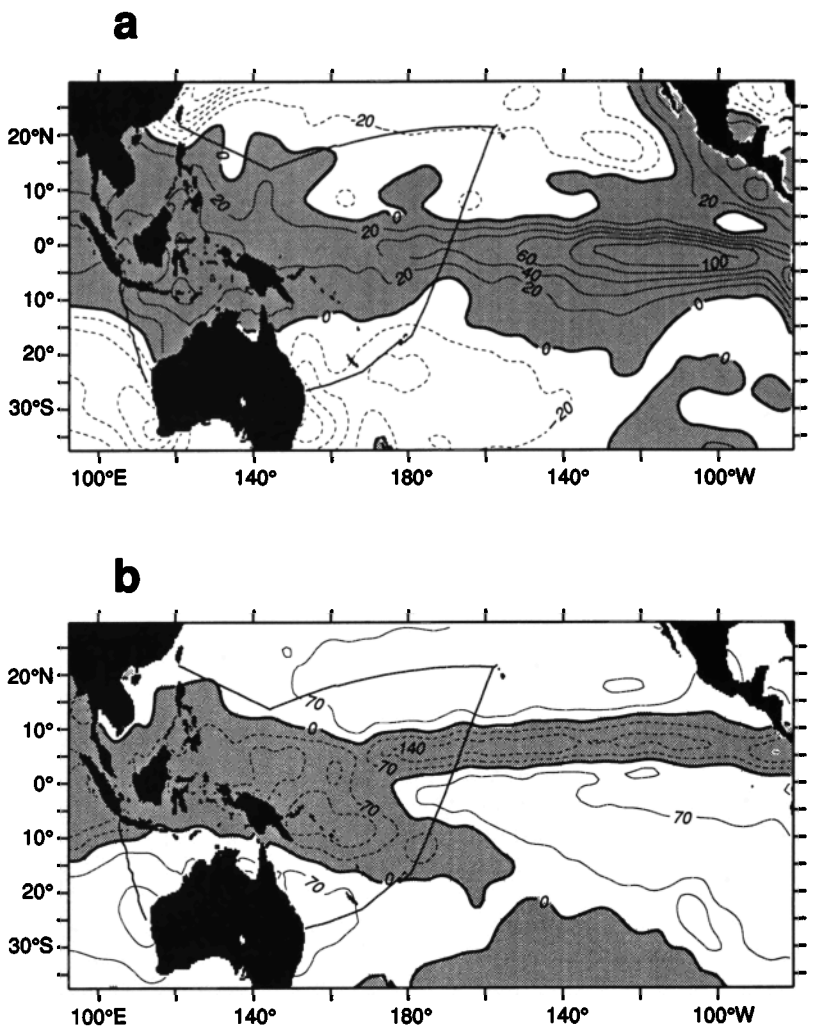

Figure 1. (a) Annual mean net surface heating [W m^{-2}]. High-resolution expendable bathythermograph (XBT) ship tracks are overlaid. Contour interval is 20 W m^{-2}. (b) Annual mean net evaporation minus precipitation [cm yr^{-1}]. Contour interval is 70 cm yr^{-1}. Both climatologies are from *da Silva et al.* [1995]. Regions of net heating and freshwater gain by ocean are shaded.

is given careful consideration in the heat and freshwater balances. These balances show a relatively shallow overturning cell comprised of dense water above $\sigma_\theta = 26$ entering the volume and more buoyant water exiting after modification by buoyancy surface fluxes. The HR XBT observations are able to resolve this cell but not the deeper cell associated with the global thermohaline circulation, which is not the focus of this study.

The sections enclose the western Pacific warm pool, which is thought to play a significant role in climate variability. Climatological heat and freshwater fluxes in this region are highly uncertain. Light winds and intense convective activity pose special difficulties for accurate surface heat and freshwater flux estimation from bulk formulae. For instance, a wide range of 20–100 W m^{-2} for equatorial western Pacific climatological heat fluxes is quoted by *Webster and Lukas* [1992]. One aim of this study is to provide residuals of oceanic heat and freshwater advection into the enclosed volume, which may be used to constrain the highly uncertain climatological surface fluxes in this region.

2. Data

HR XBT data from repeating ship-of-opportunity transects in the west central Pacific form the primary data set for this study. The data are measured as part of a World Ocean Circulation Experiment (WOCE) high-resolution XBT program aimed at the low-frequency variability of oceanic general circulation over a wide range of spatial scales. Accurate estimates of zonal fluxes across the section are allowed by the eddy-resolving sampling strategy, ~35 km midtrack and ~10 km over continental shelf areas and in the equatorial band. Temperature is measured to a depth of 800 m at quarterly intervals. Cruise information is summarized in Table 1.

The northern, southern, and eastern legs are shipping tracks where HR XBT data are available. Additional cruise information for these three sections is available from *Sprintall et al.* [1996]. Salinities (S) are obtained from temperature (T) using a spatially varying estimate of the annual mean T/S, produced by objective mapping of the National Oceanographic Data Center (NODC) hydrographic data. Additionally, about one

third of the cruises between Fiji and Hawaii have directly measured salinities using expendable conductivity-temperature-depth probes (XCTD). The direct measurements are particularly useful in the surface layer where there is no tight relation between temperature and salinity, so that salinity estimates have a relatively high uncertainty. This source of error for XBT-derived heat and freshwater fluxes will be discussed further when the advective fluxes and their uncertainties are presented. XCTD resolution is sparse along track but is strategically more concentrated within the tropical band with about 10 probes dropped between 5°S and 5°N. Where available, directly measured salinities are merged with the statistically estimated salinity.

Collection and processing of data along the western Indian Ocean leg are discussed by *Meyers et al.* [1995]. Temperature sections were collected using XBT probes from volunteer observing ships as part of the Tropical Ocean–Global Atmosphere (TOGA)/WOCE XBT network. However, sampling and data processing differ from the HR XBT program. Along-track spatial resolution is reduced (~100 km), but temporal coverage is greater with >18 cruises a year after 1987. Mean temperature sections were prepared to a depth of 800 m for overlapping bimonths by averaging in 1° latitude and 1°–3° longitude bins along the transect. The end point bins include data from 2° latitude bins owing to reduced meridional data coverage. Salinity estimates are calculated as for HR XBT data.

Density estimates are converted to vertical velocity shear using thermal wind, and velocity is obtained by referencing to 800 m (or the bottom depth if shallower than 800 m). The sensitivity of the circulation to reference level adjustments and the effect that these have on the advective budgets is an important issue which is considered in section 6. The description of each section begins with the meridional track between Fiji and Hawaii. As this is the section that samples zonal currents transporting heat across the central Pacific, the description is more detailed than the other sections that close the western/central Pacific box region.

3. XBT Observations

3.1. Eastern Section: Fiji–Hawaii

The meridional central Pacific section spans subtropical and tropical regimes, sampling the equatorial band where currents are swift, variable, and spatially complex. Plates 1a and 1b show the 8-year mean temperature and salinity, respectively, with mean velocity in Plate 1c overlaid with mean σ_θ. The westward flowing branches of the North and South Pacific subtropical gyres are apparent as a gradual rise of the isotherms, as the equator is approached from Fiji (18°S) and Hawaii (21°N). Any particular temperature snapshot shows strong small-scale features, but these have generally been removed by temporal averaging. The surface temperature minimum due to upwelling clearly locates the equator. Warmest surface temperatures appear about 500 km poleward of this minimum, roughly underlying the atmospheric South Pacific and Intertropical Convergence Zones.

The use of geostrophy to infer velocity is controversial close to the equator. In fact, the credibility of the box calculation rests to a large extent on validity of the geostrophic equatorial transports. For this reason a subsection is included to describe the equatorial geostrophic technique. The mean equatorial velocity will be shown to agree very well with a direct nearby measurement.

Table 1. Cruise Information

Leg	End Points	Time Span	Cruise Total	Probe Total
North	Taiwan and Hawaii	1991–1995	14	~230
East	Fiji and Hawaii	1987–1995	31	~150
South	Brisbane and Fiji	1991–1995	18	~100
West	Shark Bay and Sunda Strait	1983–1994	>100	~20

3.1.1. Equatorial geostrophy: Background and technique. Zonal velocity shear u_z is not measured and must be inferred from the density field using the thermal wind equation,

$$\rho_0 f u_z = -g\rho_y, \tag{1}$$

where ρ is the deviation from the mean density ρ_0, g is the gravitational acceleration, and $f = 2\Omega \sin y$ is the Coriolis parameter. Conventional midlatitude calculations of geostrophic shear from meridional density gradients cannot be accurately applied close to the equator. This is because the geostrophic contribution to the density field (right-hand side of (1)) becomes so small as $f \to 0$ that it is swamped by measurement error and ageostrophic terms not included in the balance.

The problem of estimating geostrophic shear from hydrographic measurements has been investigated by several authors (see *Picaut and Tournier* [1991] for a recent review). These studies suggest that the meridional scale of the mean geostrophic velocity field is large enough to allow interpolation within about 1° of the equator, where the signal to noise ratio is low. However, estimates of equatorial shear are sensitive to the chosen form of data smoothing used to suppress noise terms, which include measurement error as well as unresolved ageostrophic terms. A new method, presented by *Cornuelle et al.* [1993] (hereinafter referred to as CMR), was developed to estimate geostrophic velocity at the equator from HR XBT sections. The geostrophically balanced part of the density field is estimated by objective mapping rather than curve fitting so as to quantify smoothing assumptions. Velocity shear is the unknown which is estimated from noisy density observations. Provided that the statistics of velocity and density noise are known, an estimate of velocity shear can be obtained as a combination of the density observations. The time mean geostrophic shear is estimated from the mean density field at each depth. The velocity shear variance function was assumed to be Gaussian at all latitudes and depths with a latitudinal e-folding scale of 150 km. Noise levels were estimated by considering internal wave displacements, rms depth uncertainty due to XBT fall rate error, and T/S error. The ratio of rms velocity shear to density uncertainty varied with depth but not latitude. The reader is referred to work by CMR and *Morris* [1996] for additional mapping details and for a discussion of assumptions and sensitivity of the velocity estimate.

Although designed to address the low signal to noise problem at the equator, the mapping method can also be used for off-equatorial sections, where it reproduces traditional calculations and is relatively insensitive to statistical assumptions. The equatorial velocity is merged with the off-equatorial estimate between 4° and 2° latitude on each side of the equator. The two are mapped separately because of a change in scale away from the equator.

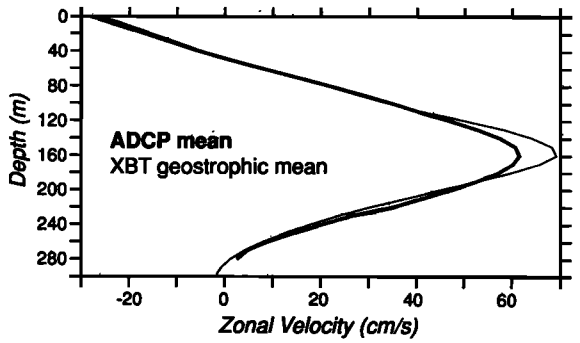

Figure 2. A comparison of the 1987–1995 mean zonal component of the cross-track geostrophic velocity (cm s^{-1}) at 170°W deduced from quarterly XBT measurements, with a nearby equatorial acoustic Doppler current profiler (ADCP) zonal velocity record [*Weisberg and Hayes*, 1995] averaged between 1988 and 1995.

3.1.2. Comparison of direct and geostrophic equatorial velocity. It is important to establish how accurately the mean geostrophic currents represent the actual velocity field. Are there sufficient measurements to allow the mean signal to be extracted from the (hopefully independent) noise? This question is examined by comparison of the mean geostrophic velocity with a nearby direct measurement.

Subsurface velocity observations are relatively sparse in the region between the western Pacific warm pool and the eastern Pacific cold tongue. To address this issue, an upward looking acoustic Doppler current profiler (ADCP) and a surface Autonomous Temperature Line Acquisition System (ATLAS) mooring have been installed at 0°, 170°W as part of the TOGA/Tropical Atmosphere-Ocean (TAO) buoy array [*Weisberg and Hayes*, 1995] (hereinafter referred to as WH) [*Weisberg and Wang*, 1997]. The site has been monitored since May 1988, providing a continuous long time series of upper ocean velocity. Data acquisition and processing are fully described by WH. Surface shear above 30 m has been linearly extrapolated using shear between 30 and 40 m. The comparison between the mean zonal component of the cross-track geostrophic velocity at the equator and the mean ADCP zonal velocity is shown in Figure 2. Agreement is excellent considering the problems associated with velocity estimation at the equator. The HR XBT geostrophic and ADCP mean velocities differ by 9%.

3.1.3. Mean circulation. Subtropical gyre flow is evident in the northern and southern parts of the mean velocity section (referenced to 800 m) shown in Plate 1. The swift currents in the equatorial band are well established and appear in any climatology of the west/central Pacific [e.g., *Wyrtki and Kilonsky*, 1984; *Delcroix et al.*, 1992; *Gouriou and Toole*, 1993]. The prominent Equatorial Undercurrent (EUC) attains a maximum eastward speed of 65 cm s^{-1} at this longitude (170°W). Geostrophic current transports estimated from this mean flow estimate compared favorably with other well-known climatologies spanning a wide region of the tropical Pacific [*Morris*, 1996].

The spatial distribution of upper 800 m transport between Fiji and Hawaii is displayed in Figure 3a. Cumulative upper 800 m transport from Fiji shows a steady accumulation of westward transport moving northward from Fiji with especially rapid change in the equatorial branch of the South Equatorial Current (SEC) near 5°S. The South Equatorial Countercurrent (SECC) can be seen as a plateau in the transport accumulation around 10°S. Just south of the equator, the South Subsurface Countercurrent (SSCC) transport manages to reverse the strong westward trend due to the SEC. Eastward flows dominate the transport from the equator to the poleward edge of the North Equatorial Countercurrent (NECC) until a reversal occurs in the westward flowing North Equatorial Current (NEC).

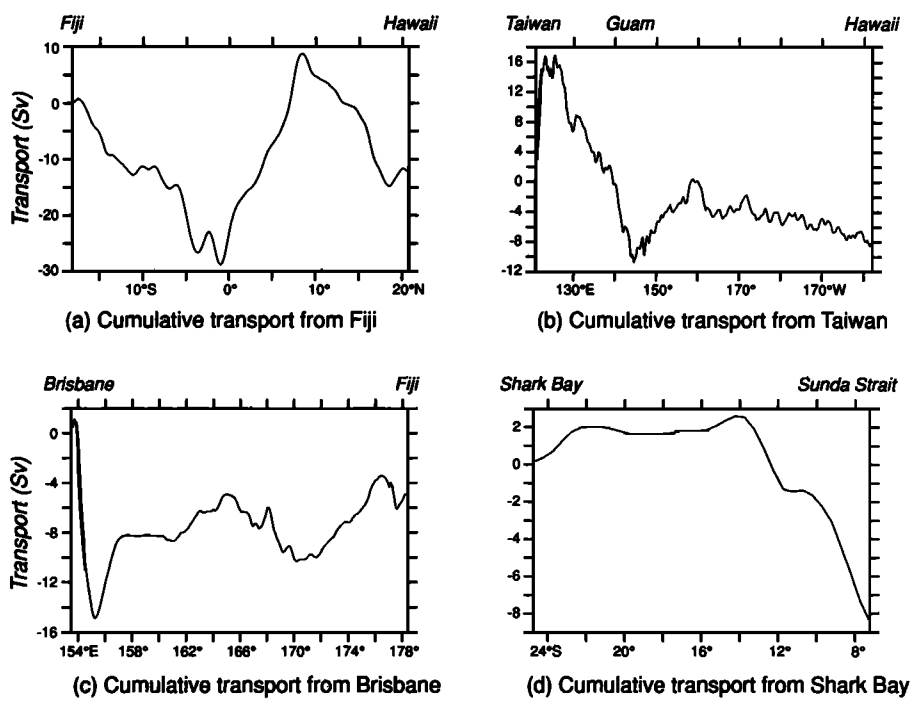

Figure 3. Cumulative upper 800 m mean transport (sverdrups) along the four sections bounding the western/central Pacific box. Northward (eastward) transport is positive across zonal (meridional) sections.

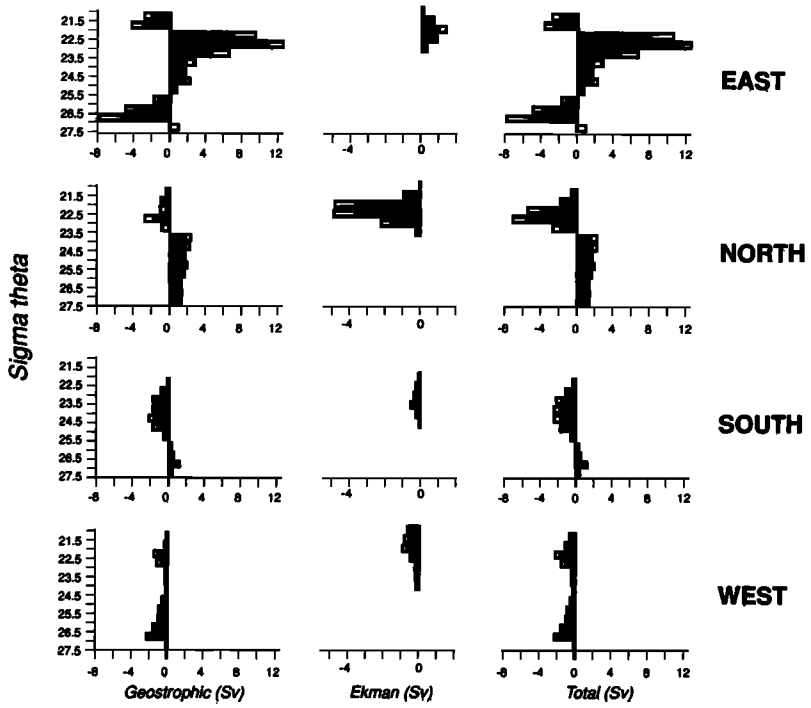

Figure 4. Mean transport (sverdrups) in σ_θ class across the four sections bounding the Pacific box. The leg is indicated by text in the last column. Geostrophic transport across each section is shown in the left column. Ekman transport computed from Florida State University (FSU) winds is displayed in the second column, and the sum of the first two columns is shown in the third column. The sign convention is positive if water is transported into the box. Open rectangular extensions indicate transport error.

3.1.4. Transport uncertainties. The total upper 800 m transport between Fiji and Hawaii is 12.7 Sv westward. The standard error for off-equatorial transport (excluding values equatorward of 3°) is 3.5 Sv. Uncertainty for the equatorial currents is estimated in two latitudinal bands: near equatorial (1°S to 1°N) and equatorial (1°–3°S and 1°–3°N). The mean fractional difference (9%) between the direct and geostrophic velocity on the equator is chosen to represent the uncertainty in near-equatorial transport. Discrepancies between the smoothed density from which the geostrophic velocity is calculated and the observed density are largest about 1°–2° off the equator, suggesting that the velocity uncertainty may increase in that latitudinal band. Closer agreement between the geostrophic and measured density can be obtained by reducing the decorrelation scale for the velocity shear. The sensitivity of the upper 800 m transport to varying decorrelation lengths was investigated, and this led to a 16% error for transport between 1°–3°S and 1°–3°N.

One limitation of the XBT monitoring program is the lack of high-resolution salinity measurements. This could introduce a systematic bias in geostrophic velocity, especially in the equatorial band. Comparison between the salinity estimate incorporating XCTD observations and the climatological salinity shows that the climatological estimate is too salty in the upper 100 m and too fresh in the upper thermocline ($z > 300$ m). Section-averaged rms differences in the upper 100 m (100–200 m) are 0.05 (0.03). This has an appreciable effect on the equatorial geostrophic flow producing rms velocity differences of ~ 5 cm s^{-1} at the surface. Transport between 5°S and 5°N was recalculated using a new salinity climatology based only on XCTD observations. This climatology may more accurately reflect mean conditions during the experiment than the climatology based mainly on historical data; however, it is limited by the number of observations. In any σ_θ band, transports may differ by 20% from the previous estimate, but the discrepancy is less when summed over all density bands, i.e., -11.9 Sv using "XCTD T/S" compared with -12.7 Sv.

The choice of a reference level at 800 m was imposed by the data and is a significant but unknown source of uncertainty in transport estimates as there may be appreciable flow at 800 m. The no-motion assumption is especially problematic close to the equator. The effect of deep flows on the heat and freshwater balances is considered by adjusting reference level velocities around the edges of the enclosed volume. These circulation adjustments (discussed in section 6.2) help quantify the uncertainty that arises from incomplete sampling of the water column.

3.2. Northern Section: Taiwan-Guam-Hawaii

Cumulative upper 800 m transport along the long nearly zonal section forming the northern boundary of the box is presented in Figure 3b. This transect samples the intense Kuroshio, which acts as a pathway for the export of heat from the tropics to the midlatitudes. The western boundary current is obvious as northward transport pressed close to Taiwan, and southward interior gyre flow is evident across the rest of the section. Recall that the transect is not purely zonal, so that westward flow in the North Pacific subtropical gyre has a northward/southward contribution to cross-track transport to the east/west of Guam. The cross-track transport of water warmer than 12°C in the Kuroshio is around 14 Sv at this latitude. This compares well with an estimate based on histor-

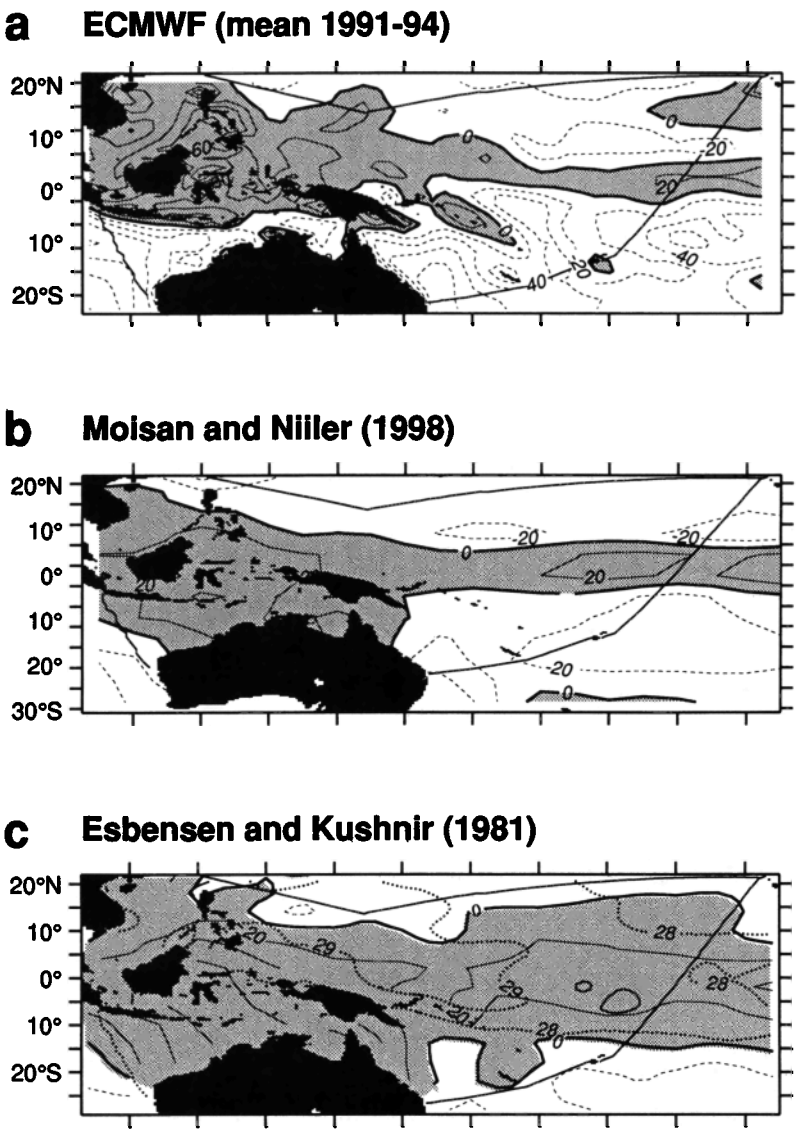

Figure 5. Estimates of net surface heating (W m^{-2}) over the western Pacific region bounded by XBT ship tracks (overlaid). The mean position of the 28° and 29°C isotherms from *Levitus* [1982] sea surface temperature climatology are contoured over *Esbensen and Kushnir*'s [1981] heat flux (Figure 5c). Figure 5b shows *Moisan and Niiler*'s [1998] climatology. Operational model output from ECMWF, averaged between 1991 and 1995, is shown in Figure 5a. Contour interval is 20 W m^{-2}, and positive values indicate oceanic heating.

ical hydrographic data between 18° and 20°N by *Toole et al.* [1988], who found 15 Sv of northward transport for waters warmer than 12°C.

There is a total of 8.3 Sv southward transport between Taiwan and Hawaii with a standard error of 1.3 Sv. Data have only been collected over a 4 year period, which encompassed a strong El Niño in the tropical Pacific. Unresolved interannual fluctuations may be aliased into the mean. NODC historical

Table 2. Integrated Climatological Surface Heat Fluxes

	$T > 29$°C		$T > 28$°C		Total	
	Surface, PW	Average, W m^{-2}	Surface, PW	Average, W m^{-2}	Surface, PW	Average, W m^{-2}
Esbensen and Kushnir [1981]	0.13	20	0.43	21	0.56	18
Oberhuber [1988]	0.22	32	0.56	27	0.56	17
da Silva et al. [1995]	0.14	20	0.44	21	0.44	14
Moisan and Niiler [1998]	0.03	5	0.07	4	0.02	1
ECMWF (1991–1994)	−0.01	−1	0.06	3	−0.15	−5

Surface, surface heat flux values integrated over a region; average, average heat flux values over the same region. Positive values indicate oceanic heating. All given numbers are mean values.

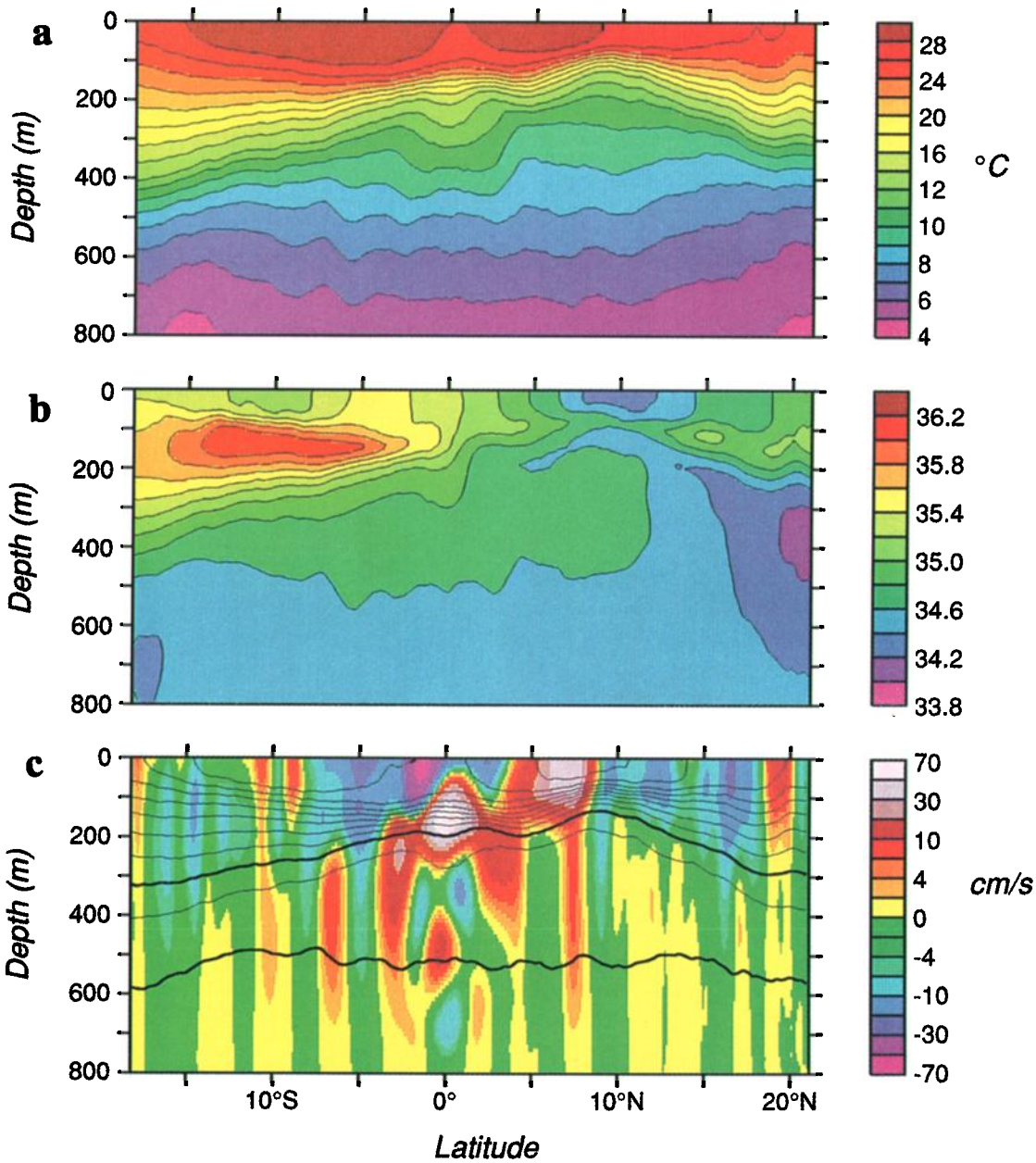

Plate 1. (a) Mean temperature, (b) salinity, and (c) the zonal component of the cross-track geostrophic velocity from quarterly XBT cruises along a repeating track between Fiji and Hawaii from 1987 to 1995. Here σ_θ is overlaid on the velocity plot with a contour interval of 0.5 and σ_θ = 26, 27 heavily shaded. Positive flow is eastward.

data along the HR XBT track were examined for evidence of long-term transport changes. Interestingly, the integral of upper 800 m transport between Taiwan and Hawaii estimated from historical data is very similar, implying that the upper 800 m transport for the period 1991–1995 is representative of a long-term mean.

The reference level is a serious issue for this section as it is clear from isotherm slopes (not shown) that geostrophic shear is not zero at the lowest sampling depth, especially close to Taiwan. Sensitivity of the upper 800 m transport to the assumed reference level was investigated using hydrographic data from a transpacific section along 24°N. Transport between the coast and 158°W along 24°N was calculated for σ_θ bands above 27.5 using a variety of reference levels. Shifting reference level resulted in changes to the upper 800 m mass and temperature transport of ~15% of the mean value. Lacking any better estimate, the same sensitivity to mid-ocean reference level is assumed along the HR XBT transect giving a relatively low error of 1.4 Sv.

3.3. Southern Section: Brisbane-Fiji

Cumulative upper 800 m transport across the southern section is shown in Figure 3c. The east Australian boundary current is evident at the western edge of the section. Substantial recirculation of this current can be seen. There is very little change in slope of the cumulative transport in the center of the section where flow is weak. The ship transect passes over major topographic features, in particular, the Lord Howe Rise close

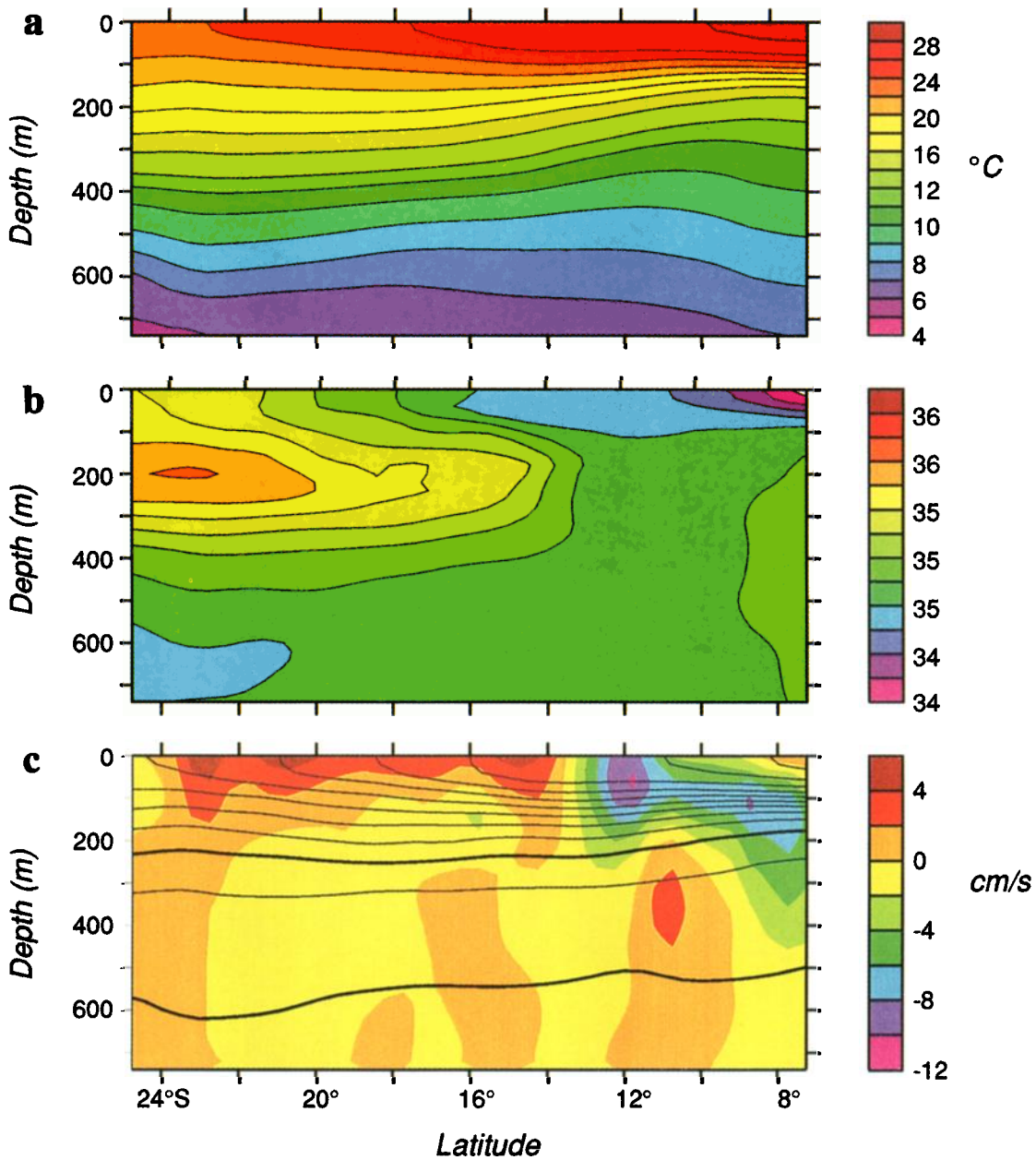

Plate 2. (a) Mean temperature, (b) salinity, and (c) the zonal component of the cross-track geostrophic velocity from XBT cruises along a repeating track between Shark Bay, Australia, to Jakarta, Indonesia, from 1983 to 1994. Here σ_θ is overlaid on the velocity plot with a contour interval of 0.5 and σ_θ = 26, 27 heavily shaded. Positive flow is eastward.

to New Caledonia (around 168°E), before veering northward to Fiji. This results in interesting midtrack velocity structure. Northward flow is seen between the East Australian Current and New Caledonia turning to southward transport over the Lord Howe Rise. The change in slope ~170°E is due to a change in track angle, where westward flow in the gyre is interpreted as northward cross-track transport. The total transport above σ_θ = 27.5 is relatively weak with 4.4 ± 0.9 Sv of southward flow. Vertical distribution of transport (not shown) is simple with southward flow of ~7 Sv above σ_θ = 26 [e.g., *Bailey et al.*, 1993] and with ~3 Sv northward flow below that.

The same concerns of short sampling period and shallow reference level for the northern leg apply to this southern section. Historical hydrographic data (including XBTs) were used in an inverse calculation by *Ridgeway and Godfrey* [1994] to develop a climatology of the Tasman Sea region. Mean transport estimates are given along zonal and meridional lines, none of which coincide with the HR XBT track; thus quantitative comparison of transport is not useful. A single CTD section between Australia and New Zealand was used to estimate transport along 30°S by *Chiswell and Stanton* [1995]. They quote a 2 Sv underestimation of southward flow for a reference level at 800 m rather than 2000 m.

3.4. Western Section: Shark Bay–Sunda Strait

A western section in the Indian Ocean closes the western Pacific box region. Upper ocean mean temperature, salinity, and geostrophic velocity are displayed in Plate 2. Eastward

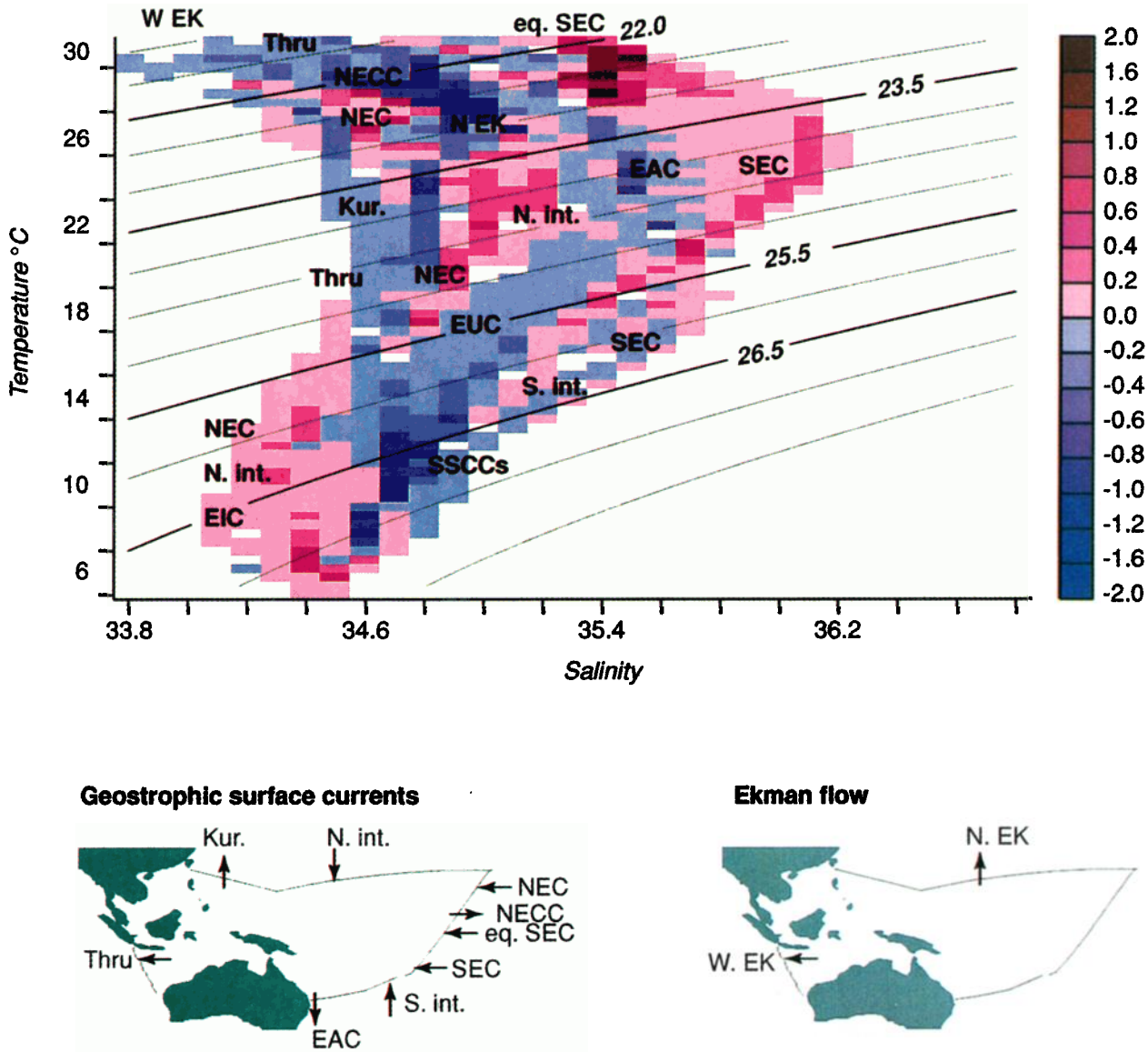

Plate 3. Mean net transport convergence (sverdrups) in the western Pacific box in temperature and salinity bins, a two-dimensional perspective. Positive values indicate a net convergence within the layer. Surface positions of the currents labeled in top section of Plate 3 are indicated schematically in the bottom section.

flow is positive. The mean thermal structure was first presented by *Meyers et al.* [1995]; this plot shows the extended data down to 740 m. Below 740 m, temperature data are scarce, so the reference level velocity has been shifted from 800 to 740 m. Isotherms display a bowl shape between Shark Bay (~25°S) and Sunda Strait (~6°S) associated with eastward flow to the south and westward flow to the north. Part of this flow is the eastern corner of the south Indian subtropical gyre. There is also net westward outflow, which is generally located to the north of the hydrological front around 14°S [*Fieux et al.*, 1994] and is particularly apparent in the cumulative upper 740 m transport from Shark Bay shown in Figure 3d. At the northern edge, eastward shear at the surface is associated with the highly variable fresh South Java Current pressed against the coast [e.g., *Meyers et al.*, 1995]. Weak westward shear at the southern edge is the signature of the Leeuwin Current, which flows generally southward along the west Australian coast.

The net upper 740 m transport across the section is 8.4 Sv. *Meyers et al.* [1995] provide a discussion of the random and systematic errors for the net transport integrated to 400 m. They suggest a mean transport error of 1–2 Sv due to not resolving the narrow Leeuwin Current. Random aliasing errors due mainly to interannual and mesoscale variability were <1 Sv for the long-term mean. A 1 Sv bias transport error was estimated because of a lack of direct salinity measurements in the South Java Current. *Meyers et al.* [1995] found that upper 400 m transport values of the Indonesian Throughflow were highly sensitive to choice of reference level. *Fieux et al.* [1996] suggest 1300 dbar as a reference depth on the basis of a water mass transition from Banda Sea Water to Deep Indian Ocean Water. Their transport plots from the Java Australia Dynamic Experiment (JADE) 92 cruise imply an average velocity of 0.1 cm s^{-1} in the 750–850 m depth range, which produces a contribution of 1.5 Sv to the upper 740 m.

The combined error for the upper 740 m transport is 2.9 Sv. The Indonesian Throughflow transport of 8.4 ± 2.9 Sv is well

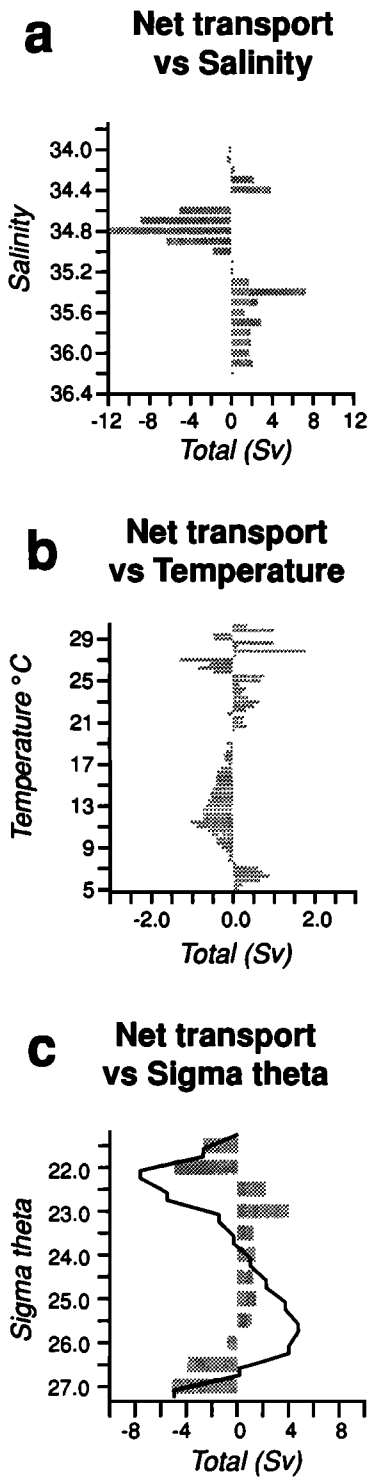

Figure 6. Net transport convergence (sverdrups) in the western Pacific box for layers bounded by (a) salinity, (b) temperature, and (c) σ_θ. The cumulative transport from the surface is contoured as a solid line. Positive values indicate a net convergence within the layer.

within the range of transports (0–20 Sv) estimated by direct or inverse methodology (e.g., see *Wijffels* [1993] for a recent review).

4. Ekman Transport

In regions of strong winds, substantial Ekman transport may dominate heat and freshwater transport by geostrophic currents. Ekman transport along the HR XBT transects is computed using two different wind products. The Florida State University (FSU) wind product converts ship data to monthly averaged, subjectively analyzed values of pseudostress $\tilde{u}|u|$. The *Large and Pond* [1981] drag coefficient is used to convert to wind stress. The ECMWF product is a model-based analysis which assimilates surface marine data as well as satellite data such as wind estimated from cloud track motion. Along the eastern leg, Ekman transport is not extended equatorward of 4°S because of the singularity at the equator. The close agreement between geostrophic and directly measured mean shear (see Figure 2) at the equator suggests that a relatively small error is associated with the neglect of mean equatorial Ekman transport.

FSU-derived Ekman transports along the four legs are shown in the middle column of Figure 4 in σ_θ classes. Strong trade winds produce substantial Ekman transport across the zonal northern leg. Ekman transport is smaller across the other lines, although it is comparable to geostrophic flow across the western leg. Transport was assumed to be uniformly distributed over the top 50 m. Uncertainty in the vertical penetration of Ekman transport is a source of error for the heat and freshwater transported by Ekman flow. This was investigated by varying the penetration depth from 10 to 100 m. The resultant errors are overshadowed by the uncertainty in the wind stress, which is difficult to determine. ECMWF and FSU Ekman transport values agreed within 20%. A recent source of wind stress derived from satellite scatterometry provides frequent measurements with global coverage. Comparison of satellite-derived winds with subjectively analyzed and operational wind products produces spatially averaged rms differences of ~0.01–0.02 N m^{-2} in the tropical Pacific for mean stress values of 0.03–0.08 N m^{-2} [*Busalacchi et al.*, 1993; *Rienecker et al.*, 1996]. Assuming this approximates the combined effect of methodology, sampling, measurement error, and data type leads to ~30% error in the annual mean wind stress. This translates to a 30% error in the mean Ekman transport calculation assuming that the wind stress error term is dominant.

5. Surface Fluxes

5.1. Heat Flux

In Figure 5, three heat flux climatologies for the Pacific Ocean demonstrate the degree of uncertainty between different estimates. Operational model output from ECMWF is shown in Figure 5a. Output is averaged from 1991 to 1994 and not the full time span of the HR XBT experiment, because of a heating trend from 1989 to 1990 which may have been caused by operational changes [*European Centre for Medium-Range Weather Forecasts, (ECMWF)*, 1993]. The annual mean climatology of *Moisan and Niiler* [1998] (hereinafter referred to as MN), shown in Figure 5b, compared seasonal heat storage in the upper ocean with variations of surface heat flux in order to choose the best fit bulk formulations. This estimate also used remotely sensed cloud data from 1983 to 1991 and a radiative transfer model to calculate solar shortwave radiation (J. Moisan, personal communication, 1996). An older estimate by *Esbensen and Kushnir* [1981] is shown in Figure 5c.

Surface heat fluxes integrated over the surface area enclosed by the HR XBT tracks and sea surface temperature contours are summarized in Table 2. Only climatologies with relatively modest heat flux into the warm pool are considered consistent with recent suggestions that older climatologies overestimated

Table 3. XBT-Derived Heat and Freshwater Divergences in the Enclosed Western Pacific Volume

Adjustment	Upper Layer	Lower Layer
	Heat Divergence, [PW]*	
1	0.02 ± 0.3	0.19 ± 0.1
2	−0.06 ± 0.3	0.13 ± 0.1
3	−0.03 ± 0.3	0.25 ± 0.1
4	−0.08 ± 0.3	0.13 ± 0.1
	Freshwater Divergence,† [Sv]	
1	0.7 ± 0.1	−0.13 ± 0.04
2	0.6 ± 0.1	−0.06 ± 0.04
3	0.7 ± 0.1	−0.15 ± 0.04
4	0.6 ± 0.1	−0.13 ± 0.04

Values are listed for four different circulation schemes in both the upper and lower layer. These divergences do not include unmeasured fluxes through the sea surface.

*Climatological surface fluxes range from 0.6 to −0.2 PW.

†Climatological surface fluxes range from 0.3 to 1.1 Sv.

heating in this region [*Bradley et al.*, 1991; *Godfrey et al.*, 1991; *Gent et al.*, 1991]. The integrated heat fluxes into the warm pool are especially low (<5 W m^{-2}) for the ECMWF and MN climatologies. These can be compared with estimates from *Weare et al.* [1981], which have average heating in that region closer to 50 W m^{-2}. Weak net oceanic heating in the warm pool from ECMWF should be viewed with caution. Directly measured heat fluxes from a buoy located in the warm pool were compared with ECMWF analyses by *Weller and Anderson* [1996]. They found significant differences; in particular, latent heat was consistently overestimated relative to buoy fluxes.

The climatologies differ over the cooler regions of the ocean also. For instance, there is very little heat lost to the atmosphere in the East Australian Current for the *Esbensen and Kushnir* [1981], *Oberhuber* [1988], and *da Silva et al.* [1995] climatologies in contrast to the MN and ECMWF climatologies. The net integrated surface heat flux over the area bounded by the HR XBT tracks is close to zero for the MN and ECMWF climatologies and shows a heat gain (0.44–0.56 PW) for all other climatologies listed in Table 2.

Error estimates for heat flux climatologies are poorly determined and are likely to be spatially dependent [*Weare*, 1989]. Systematic differences between the climatologies due to different processing, treatment of clouds, and choice of bulk parameterizations can be large [e.g., *Talley*, 1984; *Blanc*, 1985]. A low value for the systematic error in heat flux would be 10 W m^{-2} [*Talley*, 1984], which corresponds to an uncertainty of ~0.3 PW when integrated over the surface of the enclosed region assuming no sign or magnitude change in the bias error.

5.2. Freshwater Flux

Large net freshwater fluxes into the ocean (up to 200 cm over a year) can be seen in the climatological estimate from *da Silva et al.* [1994] shown in Figure 1b. There is a net loss of water from the ocean to the atmosphere over the subtropics and the east Pacific cold tongue. Two estimates of the net freshwater flux integrated across the surface bounded by XBT tracks are 0.3 Sv [*da Silva et al.*, 1995] and 1.1 Sv [*Oberhuber*, 1988]. In both cases, evaporative fluxes and precipitation rates were derived from bulk parameterizations using historical marine data and suffer from the usual uncertainties of this method. Here *da Silva et al.* [1995] attach a high 50% error to this type of rainfall estimate.

The distribution of net freshwater flux over the 1987–1994 period is quite likely altered from the climatology shown in Figure 1b. El Niño–Southern Oscillation (ENSO)-related shifts in the tropical Pacific precipitation field have been observed [e.g., *Janowiak and Arkin*, 1991; *Spencer*, 1993]. A 15 year time series of rainfall obtained from seven National Oceanic and Atmospheric Administration (NOAA) satellites using microwave sounding units (MSU) is available to estimate the interannual variability R. W. Spencer and V. L. Griffin, A TOVS Pathfinder path C product, Daily 2.5 degree gridpoint layer temperatures and oceanic rainfall for 1979–93, 1994) (available at http://ingrid.ldeo.columbia.edu/SOURCES/.NASA/.msu/.dataset_documentation.html). Rainfall data were spatially integrated between 120°E and the date line, equatorward of 20°, and averaged over two periods: the entire period of MSU data 1979–1994 and the HR XBT experiment span between 1987 and 1994. Differences in the integrated rainfall between the two time periods were negligible (<5%) relative to uncertainty.

6. Mean Balances

6.1. Unadjusted Circulation

Mean geostrophic transports in σ_θ classes are summarized in the first column of Figure 4 along all four legs bounding the western Pacific box. Ekman and net transport are shown in the second and third columns, respectively. Figure 4 shows that a significant part of the shallow mass balance will be between geostrophic inflow through the eastern side of the box and Ekman outflow across the northern section. Important contributions are also due to geostrophic outflow along the southern leg and combined Ekman/geostrophic transport to the Indian Ocean.

Net transport convergences for each density layer obtained by summing transports around the four sides of the box are displayed in Figure 6c. The cumulative transport from the surface downward is also contoured. Two vertical overturning cells with zero mass divergence are evident. In the lightest density range ($\sigma_\theta < 23.5$), net outflow is compensated by relatively shallow denser inflow. A second complete cell lies between $23.5 < \sigma_\theta < 26.5$ with shallow inflow compensated by outflow at an even denser range implying downwelling within the cell. The unadjusted circulation (with zero reference level velocity) predicts a relatively shallow surface interacting cell ($\sigma_\theta < 23.5$) with no contribution to the surface heat and freshwater balances from flow in denser water classes. It will be seen in section 6.2 that the vertical extent of the surface interacting cell and hence the contribution of deeper currents will vary with different circulation patterns arising from reference level flow adjustments. It is worthwhile considering the unadjusted circulation first bearing in mind that this is but one of many possible solutions.

6.1.1. Surface interacting cell $21 < \sigma_\theta < 23.5$. Summing from the surface over the shallow density bands gives 7.6 Sv net outflow in the range σ_θ = 21–22, balanced by 7.6 Sv inflow between σ_θ = 22 and 23.5. Density surfaces above σ_θ = 23.5 outcrop within the enclosed volume, so part of the modification of relatively dense inflowing water to light outflow may be due to surface fluxes. It is natural to assume that heat gain through the surface is responsible for much of the conversion of dense to light water. However, that is not true for this case. Water freshening by surface freshwater fluxes accounts for ~70% of the buoyancy change in the upper cell, which has 7.6 Sv of inflow water converted to outflow that is on average 2°C

colder and 2 practical salinity scale units (pss) fresher than the inflow.

Considerable T/S variability within density classes allows warm salty geostrophic inflow to leave as fresh slightly cooler water. To illustrate this point further, Figures 6b and 6a also display the net transport convergences in temperature and salinity classes, respectively. There is a significant inflow of water warmer than 27°C that is partially balanced by colder outflow $T \sim 25 - 27$°C (see Figure 6b). Figure 6a shows clearly that salty water flows into the box (although there is also a weak inflow of very fresh water) and fresher water leaves the volume. To aid interpretation, a two-dimensional view is presented in Plate 3.

Net transport convergences within the western Pacific box computed in temperature and salinity bins are displayed in Plate 3. Mean σ_θ curves are overlaid, and important currents are identified with some positions shown schematically in the bottom section of Plate 3. This plot collapses to Figure 6 if transport convergences are summed over salinity, temperature, and σ_θ bands, respectively. It is apparent that water masses are modified within the volume, as net inflow and outflow appear in different T/S bands. If currents merely flowed through the region with no property modification, then Plate 3 would show regions of zero net transport where inflow balanced outflow with the same T/S properties.

There is a tendency for net inflow (red shading) to be warmer than net outflow (blue shading) within the same density class above $\sigma_\theta = 23.5$. As a result, there is net convergence of heat equal to 0.04 PW over the mass-balanced range between $\sigma_\theta = 21$ and 23.5. This points to the important influence of salinity which allows SEC/NEC water to be cooled/heated with no mass flux across isopycnals. It is pertinent to question whether this result is robust in the face of salinity uncertainty. Separation of inflow and outflow in T/S space is slightly greater using the best guess salinity estimate that incorporates direct measurements rather than the climatological salinity field. However, it is found that heat flux within density layers is not critically sensitive to the salinity estimate. A more detailed description of the upper cell, which identifies key contributions from different currents, is postponed to section 6.3.

6.1.2. Second cell $23.5 < \sigma_\theta < 26.5$. An additional convergence of 4.8 Sv occurs between $\sigma_\theta = 23.5$ and 25.5. This net inflow is compensated by net outflow of deeper water between $\sigma_\theta = 25.5$ and 26.5 where eastward flow below the EUC core and in the deep subsurface countercurrents (NSCC and SSCC) exceeds the subtropical gyre inflow. There is a heat gain of ~0.2 PW in the volume owing to the fact that inflowing warm water leaves at a lower temperature. Some of this water is cooled by interaction with the deeper ocean and not the ocean surface as the part of the conversion occurs below the densest outcropping layer. If the heat diffusivity coefficient κ is positive, this is physically plausible only when the curvature of the temperature field is negative. In this scenario the rate of change of heat following a water parcel dQ/dt is balanced by turbulent vertical diffusion of heat, i.e.,

$$mC_p dT/dt = mC_p \kappa T_{zz}, \quad (2)$$

where T is the temperature, m is the mass of the water changing temperature, and $C_p = 3990$ J K^{-1} kg^{-1} is the specific heat capacity. (Horizontal heat diffusion is neglected.)

One region where this scenario is conceivable is the equatorial band (where much of the deep divergence occurs). Curvature is negative, $T_{zz} \sim -1.5 \times 10^{-3}$°C m^{-2}, below the core of the EUC where water parcels may be cooled by diffusion as they traverse eastward across the Pacific. If the water parcel enters the equatorial band in the same temperature range that it flows into the box ($T \sim 22$°C) and exits the box with an average temperature of around 12°C, then the left side of (2) is $\sim \rho V C_p \Delta T$, where $\rho = 1000$ kg m^{-3} refers to the density and V is the transport. The middle cell involves 4.8 Sv of water decreasing temperature by 8°C, so that $dQ/dt \sim -0.2$ PW. We estimate that this cooling occurs in a narrow band of ±2° latitude centered on the equator over a zonal strip between 140°E and 170°W (the eastern section equatorial crossing), i.e., a surface area of 2.5×10^{12} m^2 and a depth range of 50–100 m. These values imply that $\kappa \sim 1$–2×10^{-4} m^2 s^{-1}.

This estimate of the vertical diffusivity coefficient is high. The heat flux associated with this strong mixing is 60 W m^{-2}, which is comparable to surface fluxes. Dissipation measurements by *Peters et al.* [1995] give heat diffusivities in the range of $\sim 5 \times 10^{-6}$ to 8×10^{-5} m^2 s^{-1} at 0°, 140°W, about 10 times lower than those required to satisfy the second cell heat balance. On the other hand, larger vertical stress divergences were noted below the core of the Equatorial Undercurrent by *Qiao and Weisberg* [1997], who used an ADCP array at 140°W to analyze the upper ocean zonal momentum balance. *Wijffels'* [1993] estimates of thermocline heat diffusivity from an inverse calculation over the equatorial Pacific were small $O(10^{-5})$ for her eastern Pacific volume, but these increased to $O(10^{-4})$ (and became more uncertain) over the western region. The unadjusted circulation is not ruled out as a possible solution, although the diffusive cooling of water below the EUC is stronger than that implied by dissipation measurements.

6.2. Circulation Adjustments

The purpose of this section is to present a few physically reasonable reference level adjustment schemes that ensure that mass is balanced in two layers: an upper layer $\sigma_\theta < 26$ and a deep layer $26 < \sigma_\theta < 27$. The lower surface $\sigma_\theta = 27$ is chosen as it lies above the deepest sampled level for all sections. Transport through the lower boundary is allowed in order that the upper ocean may interact with deeper levels. There is a net convergence of 4.2 ± 3.7 Sv in the upper layer and a divergence of 9. ± 1.7 Sv in the lower layer. The lower boundary of the upper layer was chosen to lie above the relatively large divergence (9 Sv) in the deeper water. This allows for the possibility of decoupling the upper layer mass imbalance from the lower layer. The deep divergence is more uncertain as geostrophic shears are weaker, flow is closer to the reference level, and there is no independent confirmation of deep equatorial velocity estimates below 300 m from direct ADCP measurements. The rationale for reference levels adjustments is to keep them as small and simple as possible. The aim is to establish a few plausible flow fields in order to test the sensitivity of the heat and freshwater balance.

Four circulation adjustment schemes are discussed below, and the results are tabulated in Table 3. A single value of specific heat capacity, $C_p = 3990$ J K^{-1} kg^{-1}, has been chosen to convert temperature transports to heat flux. Attempts to balance the lower-layer divergence of 9 Sv can lead to unacceptably large convergence in the upper layer. The uncertainty in Ekman transport divergence of ~5 Sv allows for flexibility in the solution which places an upper limit of ~17 Sv on the Ekman transport divergence. The first three adjustment schemes assume no interaction between the upper and lower cells, so that the cross isopycnal flux across $\sigma_\theta = 26$ is zero and

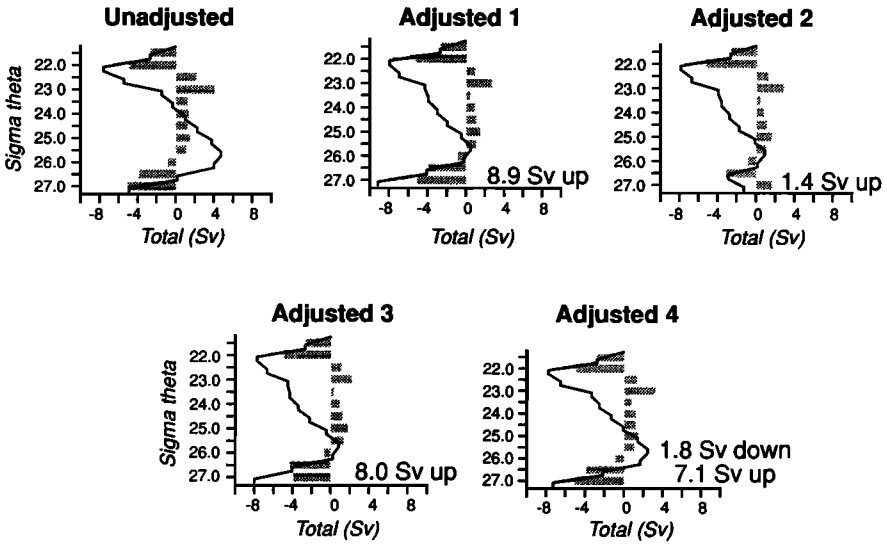

Figure 7. Mean net transport convergences [sverdrups] within σ_θ layers for different adjustment schemes (see text for details). The cumulative transport convergence integrated from the surface is overlaid. Cross-isopycnal interface transports required to balance mass in the upper layer $\sigma_\theta < 26$ and lower layer $\sigma_\theta = 26$–27 are indicated.

the more uncertain deep layer divergence is decoupled from the upper layer. The fourth adjustment allows for transport between the upper and lower layer.

The true solution may require both reference level adjustments and Ekman transport corrections (assuming that the geostrophic shears are well represented). The first adjustment isolates the effect of altering Ekman transport. Adjustment 1 increases Ekman transport divergence by a very reasonable 4.2 Sv. After adjustment, net Ekman outflow balances geostrophic inflow in the upper layer. Ekman flow increases are applied uniformly around the enclosed box. Geostrophic transports are unchanged as no reference level adjustments have been made. Total transport convergences for all adjusted circulations are displayed in Figure 7. Zero crossings of the cumulative convergence from the surface (shown as a line in the last column) indicate the vertical extent of each cell. The strong second cell of the unadjusted circulation has all but disappeared in the adjustment 1 circulation (barely visible between $\sigma_\theta = 25$ and 26) since the net convergence is now balanced by stronger outflow in a thin upper layer.

Cross-isopycnal flux is zero across $\sigma_\theta = 26$ by construction so weak downwelling is implied across $\sigma_\theta = 25.5$. Upwelling occurs over the lighter density layers. About 1 Sv of ~17°C water flows into the box between $\sigma_\theta = 25$ and 25.5 and loses heat to the deeper ocean to leave between $\sigma_\theta = 25.5$ and 26 with a temperature of ~14°C. Only a small volume of water is involved, and the implied heat diffusivities are moderate; $\kappa \sim 1 - 3 \times 10^{-5}$ m^2 s^{-1}. Lower-layer divergences are balanced by uniform vertical upwelling across the base of the lower layer ($\sigma_\theta = 27$). The downward diffusion of heat implied by the 8.9 Sv upwelling of cool water predicts a moderate value for the vertical diffusivity coefficient $\kappa = 5 \times 10^{-5}$ m^2 s^{-1} if the cross-isopycnal w is spread across the lower layer of the box.

Now consider the effects of two different reference level adjustments schemes shown in Figure 8. Reference level adjustments were assumed to be independent in seven broad zones: a boundary current and interior region for the northern and southern legs and a northern, southern, and equatorial band along the eastern leg. Any net convergences after reference level adjustments were compensated by upwelling across the lower interface in the lower layer and Ekman flow in the upper layer. Adjustment 2 reference velocities are least squares inverse solutions from an initial guess of zero reference level velocity everywhere. Adjustment 3 is an ad hoc choice which is meant as a schematic representation of the actual 800 m flow field.

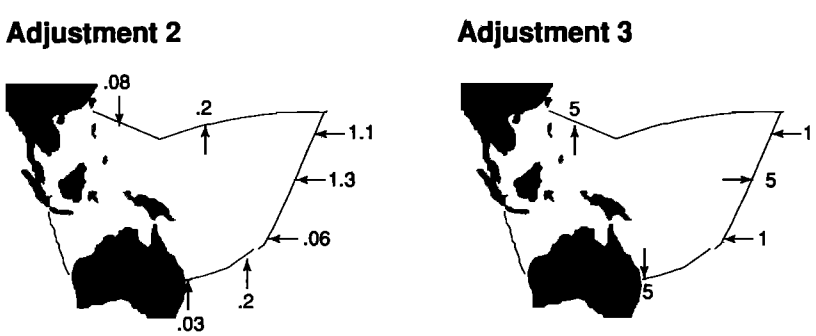

Figure 8. Reference level adjustments (cm s^{-1}) around the four high-resolution XBT sections bounding the western Pacific box. See text for details.

The least squares solution (adjustment 2) chooses broad weak westward inflow along the eastern leg and inflow through the southern boundary, which is partially balanced by an outflow through the northern section. It is worth restating that the goal of these adjustments is to investigate the sensitivity of the surface heat and freshwater balances. This is not an attempt to find the most plausible circulation pattern at the reference level. Only a weak upwelling of 1.4 Sv is required across the lower boundary as the lower-layer divergence has been nearly compensated by reference level flow convergences. This is particularly apparent in Figure 7, which shows a convergence of flow between $\sigma_\theta = 26.5$ and 27 unlike any other adjustment scheme. Total transport convergences in the upper layer are similar to adjustment 1 since intensified Ekman transports have reduced transport convergences in the range $\sigma_\theta = 22.5$–24.5. As for adjustment 1 (and also adjustment 3 discussed below), the downwelling cell of ~1 Sv at $\sigma_\theta = 25.5$ implies moderate heat loss to the lower ocean.

It appears likely that at least some of the deep layer outflow in the near-equatorial jets is balanced by broad westward reference level flow along the eastern section [*Reid*, 1986; *Reid and Mantyla*, 1978; *Tsuchiya*, 1991]. Thus the ad hoc choice (adjustment 3) brings weak westward flow into the box in the off-equatorial section of the eastern leg with mass outflow at the equator. Boundary current transports are boosted. The adjustments alone produce nearly zero mass convergence at the reference level, so an upwelling of 8 Sv is required to balance mass in the lower layer, similar to adjustment 1. As noted previously, this implies a physically reasonable value for cross-isopycnal transport. The vertical profile of total transport convergences in the upper layer is again similar to adjustments 1 and 2. (Coincidentally, net geostrophic transport convergences in the upper layer are the same for 2 and 3).

The final adjustment (adjustment 4) allows for interaction between the upper and lower cell. The entire upper layer imbalance of 4.2 Sv is not completely compensated by outflow through the lower interface as that cell would be nearly the same as the middle cell of the unadjusted circulation which had 4.8 Sv of water losing heat to the lower ocean and high implied vertical heat diffusivity. Adjustment 4 has been chosen to give less cross-isopycnal transport across $\sigma_\theta = 26$. The downwelling cell consists of 1.8 Sv of water between $\sigma_\theta = 24.5$ and 26, which flows out of the region between $\sigma_\theta = 26$ and 26.5. The diffusivity coefficient is estimated to lie in the range of $3–6 \times 10^{-5}$ $m^2 s^{-1}$ with associated heat fluxes of 10–20 W m^{-2}. The excess mass in the upper layer is removed by boosting Ekman flow across the northern leg by 2.4 Sv.

6.3. Heat and Freshwater Balances

There is no net heat divergence from the upper layer for all adjustment schemes (Table 3). The strength and vertical extent of the surface interacting overturning cell are sensitive to reference level adjustments. The very shallow cell $\sigma_\theta < 23.5$ associated with the unadjusted circulation implies strong mixing in the underlying middle cell (see section 6.1.2). The vertical extent of the surface interacting cell increased to $\sigma_\theta = 24.5$ if a small mass flux (1.8 Sv) was allowed across $\sigma_\theta = 26$ as in adjustment 4. The deepest upper cells extended to $\sigma_\theta \sim 25.5$ (adjustments 1, 2, and 3).

Deeper flows have the most uncertainty as they have the weakest shears and occur closest to the unknown reference level. It was found to be difficult to balance the lower-layer divergence using only reference level velocity adjustments as unacceptably large convergences in the upper ocean $\sigma_\theta < 26$ were produced that could not be compensated by increasing Ekman divergence. Some upwelling through the lower surface of the layer is favored. Heat was found to be divergent in the lower layer ($26 < \sigma_\theta < 27$) for all adjustment schemes. Part of this heat divergence is compensated by vertical diffusion from the layer above, which loses heat to the deeper ocean in a weak downwelling cell. Peak downward diffusion of heat occurs with the adjustment 4 circulation, which has the strongest downwelling cell between $\sigma_\theta = 24.5$ and 26.5.

While only four adjustment schemes are presented here, several others were investigated. No heat convergence over the enclosed upper volume (0 ± 0.3 PW) was seen for all adjusted circulations (provided that the constraint of reasonable diapycnal fluxes within the water column was satisfied). This result is satisfying as the total heat advected into the volume is insensitive to the arbitrary small adjustments necessary to satisfy mass constraints. Neglecting heat storage in the volume, the XBT-derived heat convergences imply zero surface heat gain or loss.

Various traditional climatological heat flux estimates through the air-sea interface predict a mean gain of heat by the ocean (0.44–0.56 PW) and contradict the HR XBT estimate of no oceanic divergence (0 ± 0.3 PW). Only the recent MN climatology, which gives zero net flux across the enclosed surface area, agrees with the XBT-derived estimate. The ECMWF model heat flux estimate averaged between 1991 and 1995 predicts a mean loss of 0.2 PW to the atmosphere in this region, which agrees with the oceanic convergence estimate within uncertainty (0 ± 0.3 PW). The HR XBT sections enclose not only the warm pool but also graze the western edge of the cold tongue, and a significant fraction of the region lies in the subtropics. It is not possible to pinpoint where the traditional heat flux climatologies might be unrealistic within the volume as the estimate predicts only an integrated value. However, high values of net heat gain in the warm pool appear to be ruled out by this direct estimate. Part of the imbalance of the climatologies with the HR XBT estimate may be due to the anomalous conditions that existed in the Pacific over the XBT sampling period. *Barnier et al.* [1995] noted that El Niño warming in the equatorial Pacific resulted in a reduction in heat gained by the ocean in the ECMWF model analyses. On the other hand, MN's estimate is based mainly on historical data, which closely balances the 1987–1995 XBT-derived estimate.

Another possibility is that the heat content of the ocean enclosed by the high-resolution XBT sections is changing. This term in the heat balance has been neglected up to now. The time rate of change of heat content in the upper 400 m of this volume has been deduced from the TOGA low-resolution XBT data set by *White* [1995]. A long time series is available through the end of 1993. Large fluctuations in the heat content of the western Pacific boxed region are observed (up to 50 W m^{-2}), but these would average to zero over a sufficiently long time period. It appears that the western Pacific volume gained 0.08 ± 0.02 PW of heat between late 1987 (the beginning of high-resolution XBT sampling along the eastern leg) and 1993. If heat content remained steady after that period, then the combined oceanic heat divergence and heat storage tendency would be 0.1 ± 0.3 PW. If heat storage in the volume continued to rise after 1993, the discrepancies between oceanic heat storage and heat transport with the climatological surface heat flux would become smaller. As an extreme example, if heat content rose to the highest level that has been recorded over

the past 14 years, it would correspond to a change of heat storage of 0.25 PW between 1987 and 1995. The combined oceanic terms 0.25 ± 0.3 PW would more nearly balance surface heat gain predicted by older climatologies 0.4–0.6 PW but would be out of range of the most recent estimate from MN.

Freshwater is gained in the warm pool region, which is an area of excess precipitation over evaporation. *Gosnell et al.* [1995] found that sensible heat loss due to differences in the temperature of raindrops and sea surface temperatures had a small effect on the steady state surface heat balance in the warm pool (<3 W m^{-2}). Strong evaporation occurs in subtropical areas, which reduces the net freshwater gain integrated over the HR XBT surface area. The HR XBT estimate of $\sim 0.7 \pm 0.1$ Sv freshwater divergence in the upper layer falls within the climatological range of freshwater input at the surface. The large surface gain of freshwater has a critical effect on the buoyancy budget of the upper ocean. Water freshening allows for conversion of dense to buoyant waters with no change in water temperature.

Which currents play important roles in the buoyancy balance? We address this question by reference to Plate 3, which shows net transport convergences of the unadjusted circulation distributed in temperature and salinity bins. (The qualitative features of this plot are unchanged for different adjusted circulations.) Transports in the North and South Pacific are clearly distinguishable by T/S properties with low-salinity North Pacific transports showing on the left side of Plate 3 and salty southern hemisphere transports on the right side of Plate 3.

Several currents contribute significantly to the upper layer buoyancy balance. Eastern Pacific water is brought into the volume by two major zonal currents, NEC and the equatorial lobe of the SEC (eq. SEC), between $\sigma_\theta = 22$ and 23.5. This inflow is partially balanced by outflow in a lighter-density range. In particular, warm and fresh waters are lost from the volume by eastward NECC flow and outflow to the Indian Ocean via the Throughflow (Thru) and Ekman flow (W. EK). Part of the large inflow in the equatorial lobe of the SEC is offset by strong Ekman outflow across the northern track (N. EK) in the same density range. Below $\sigma_\theta = 23.5$, interior subtropical gyre flows are partially balanced by western boundary currents. Thus westward SEC transport and deep northward flow across the southern boundary (S. int.) carries water into the volume, which is partially removed by the East Australian Current (EAC). The same situation applies to the northern hemisphere, where inflow from the NEC and southward interior transport across the northern leg (N. int.) flows out in the Kuroshio (Kur.). Part of the denser subtropical gyre inflow reaches the equatorial band and leaves the volume in the upper part of the Equatorial Undercurrent (EUC), and part crosses the equator to flow out of the box as cool fresh Throughflow (Thru.) waters in the same density range.

7. Conclusions

A long-term XBT/XCTD monitoring system provides well-resolved estimates of heat and freshwater fluxes in the upper 800 m across repeated transects in the Pacific. The sections bound a region of quite varied atmospheric forcing. The western Pacific warm pool, with small heat and large freshwater gain through the air-sea interface, is completely enclosed. On a larger scale, intense surface heat gain in the tropical eastern Pacific is balanced by heat loss in midlatitudes, particularly at western continental boundaries. The interplay of zonal currents in transporting water to the west and poleward flow in the western boundary currents and Ekman flow was one of the focuses of this paper.

Air-sea fluxes within the volume cannot be ignored. This means that currents do not act as insulated pipes carrying water from the eastern tropical Pacific diagonally through the enclosed volume to lose heat poleward of the box boundaries. This is evident from Plate 3, which shows inflow and outflow clearly separated in T/S space. Westward flowing SEC and NEC currents move water from the eastern Pacific toward the west where heat and freshwater may be gained through the warm pool surface. A significant fraction of inflow is returned eastward as warm fresher water in the NECC. The dominant outflow, however, is due to Ekman transport across the long northern leg. Water leaving in the Ekman layer is relatively cool having lost heat to the atmosphere prior to flowing across the northern boundary.

Some SEC and NEC water is transported through the Pacific and leaves as warm and fresh Indonesian Throughflow and Ekman transport to the Indian Ocean. While volume transport is not large, the effect on the upper layer heat and freshwater balance is noticeable because of the low salinites and high temperatures of the outflowing water. Also contributing to the surface interacting cell are cool waters exiting to the south in the EAC and eastward along the equator in the upper EUC. Upwelling waters in the EUC eventually play a dominant role in the surface heat budget of the eastern Pacific.

Mean net transport convergences show an upper ocean circulation cell with dense ($\sigma_\theta \sim 22$–26) water entering the volume and light water departing. The strength of the circulation as well as the density range of inflow and outflow depend on whichever scheme is chosen to balance mass. If no adjustments are made, then the extent of the upper cell is shallow $\sigma_\theta = 23.5$. This may be shifted to $\sigma_\theta \sim 26$ with suitable reference level and Ekman transport adjustments. A surprising result emerges regardless of the details of the circulation adjustments. No heat gain is required to convert the dense water to light water. Large freshwater gain through the surface plays a critical role in the buoyancy balance by allowing conversion of dense to light water with little change (or even a drop) in temperature. The HR XBT estimate of oceanic freshwater divergence was 0.7 ± 0.1 Sv, which was within the range predicted by two climatological estimates (0.3–1.1 Sv).

Negligible oceanic heat divergence is consistent with recent recognition that air-sea heat flux into the warm pool must be small [e.g., *Godfrey et al.*, 1991]. Modeling studies [e.g., *Gent*, 1991] and recent observational efforts aimed at better bulk formulation through comparison with direct measurements [*Webster and Lukas*, 1992] all point to a value of ~ 20 W m^{-2} over the warm pool. Most climatological estimates predict too much net heat gain through the surface (0.4–0.6 PW) to balance the combined heat storage change and heat advection into the region. Only the most recent estimate from *Moisan and Niiler* [1998] balances the XBT-derived estimate. Part of the discrepancy may be due to the anomalous meteorological conditions that prevailed in the Pacific between 1987 through 1988/1989 La Niña and the warm event(s) of 1991–1994. However, the close agreement to MN's climatology, which is mainly based on historical data, reduces the likelihood of that possibility. ECMWF operational model output between 1991 and 1994 gave a net heat loss over the western Pacific box (-0.2 PW) that agreed with the HR XBT estimate within uncer-

tainty. Whether this was due to assimilation of contemporaneous meteorological data is unclear. Large uncertainties in climatological heat flux estimates are expected. The virtue of the XBT heat divergence estimate is that when combined with heat storage information, it can be used to constrain the range of climatological surface heat fluxes.

Acknowledgments. We are extremely grateful to Blue Star Line Inc., Sea-Land Service Inc., and Forum Line Inc. and to the ship's captains and crews for their continued assistance and cooperation in the high-resolution XBT program. Data processing and collection were carried out by R. Bailey, B. Cornuelle, D. Cutchin, B. Duffy, C. Greengrove, S. Hautala, P. Jackson, L. Lehmann, M. Morris, A. Quigley, D. Roemmich, P. Sutton, W. White, C. K. Wu, and W. R. Young. This work is part of M. Y. M's Ph.D. thesis, and she wishes to acknowledge the helpful comments from committee members T. Chereskin, D. Luther, and L. Talley. Comments from N. Schneider and J. Sprintall and three anonymous reviewers also significantly improved the manuscript. This work was supported by the National Science Foundation as a component of the World Ocean Circulation Experiment through grants OCE87-10084 and OCE90-04230.

References

Bailey, R., D. Roemmich, G. Meyers, W. Young, and B. Cornuelle, Transports of the major current systems in the Tasman Sea, in *Fourth International Conference on Southern Hemisphere Meteorology and Oceanography*, edited by D. Karoly, and R. Rosen, p. 535, Am. Meteorol. Soc., Boston, Mass., 1993.

Barnier, B., L. Siefridt, and P. Marchesiello, Thermal forcing for a global ocean circulation model using a three-year climatology of ECMWF analyses, *J. Mar. Syst.*, *6*, 363–380, 1995.

Blanc, T., Variation of bulk-derived surface flux, stability, and roughness results due to the use of different transfer coefficient schemes, *J. Phys. Oceanogr.*, *15*, 650–669, 1985.

Bradley, E., P. Coppin, and S. Godfrey, Measurements of sensible and latent heat flux in the western equatorial Pacific Ocean, *J. Geophys. Res.*, *96*, 3375–3390, 1991.

Busalacchi, A., R. Atlas, and E. Hackert, Comparison of special sensor microwave imager vector wind stress with model-derived and subjective products for the tropical Pacific, *J. Geophys. Res.*, *98*, 6961–6977, 1993.

Chiswell, S., and B. Stanton, Volume and heat transports, Tasman Sea, May–June '93, *Int. WOCE Newsl. 19*, pp. 8–10, WOCE Int. Proj. Off., Southampton Oceanogr. Cent., Southampton, England, 1995.

Cornuelle, B., M. Morris, and D. Roemmich, An objective mapping method for estimating geostrophic velocity from hydrographic sections including the equator, *J. Geophys. Res.*, *98*, 18,109–18,118, 1993.

da Silva, A., C. C. Young, and S. Levitus, *Atlas of Surface Marine Data 1994*, vol. 1, *Algorithms and Procedures*, *NOAA Atlas NESDIS 6*, 83 pp., Natl. Oceanogr. Data Cent., Silver Spring, Md., 1995.

Delcroix, T., G. Eldin, M. Radenac, J. Toole, and E. Firing, Variation of the western equatorial Pacific Ocean, *J. Geophys. Res.*, *97*, 5423–5445, 1992.

Esbensen, S., and Y. Kushnir, The heat budget of the global ocean: An atlas based on estimates from surface marine observations, *Rep. 29*, 27 pp., Clim. Res. Inst., Oreg. State Univ., Corvallis, 1981.

European Centre for Medium-Range Weather Forecasts (ECMWF), The description of the ECMWF/WCRP III—A global atmospheric data archive, *Tech. Attachment ECMWF 1–18*, Reading, England, 1993.

Fieux, M., C. Andrié, P. Delecluse, A. Ilahude, A. Kartavtseff, F. Mantisi, R. Molcard, and J. Swallow, Measurements within the Pacific-Indian oceans throughflow region, *Deep Sea Res., Part I*, *41*, 1090–1130, 1994.

Fieux, M., R. Molcard, and A. G. Ilahude, Geostrophic transport of the Pacific-Indian Oceans throughflow, *J. Geophys. Res.*, *101*, 12,421–12,432, 1996.

Gent, P. R., The heat budget of the TOGA-COARE domain in an ocean model, *J. Geophys. Res.*, *96*, suppl., 3323–3330, 1991.

Godfrey, J. S., M. Nunez, E. E. Bradley, P. A. Coppin, and E. J. Lindstrom, On the net surface heat flux into the western equatorial Pacific, *J. Geophys. Res.*, *96*, suppl., 3391–3400, 1991.

Gosnell, R., C. Fairall, and P. Webster, The sensible heat of rainfall in the tropical ocean, *J. Geophys. Res.*, *100*, 18,437–18,442, 1995.

Gouriou, Y., and J. Toole, Mean circulation of the upper layers of the western equatorial Pacific Ocean, *J. Geophys. Res.*, *98*, 22,495–22,520, 1993.

Janowiak, J., and P. Arkin, Rainfall variations in the tropics during 1986–1989, as estimated from observations of cloud-top temperature, *J. Geophys. Res.*, *96*, 3359–3373, 1991.

Large, W., and S. Pond, Open ocean flux measurements in moderate to strong winds, *J. Phys. Oceanogr.*, *11*, 324–336, 1981.

Levitus, S., Climatological atlas of the world ocean, *NOAA Prof. Pap. 13*, 173 pp., U.S. Gov. Print. Off., Washington, D. C., 1982.

Meyers, G., R. Bailey, and A. Worby, Geostrophic transport of Indonesian Throughflow, *Deep Sea Res., Part I*, *42*, 1163–1174, 1995.

Moisan, J., and P. Niiler, The seasonal heat budget of the North Pacific: Net heat flux and heat storage rates [1950–1990], *J. Phys. Oceanogr.*, in press, 1998.

Morris, M., Mean and low frequency fluctuations in the circulation of the western/central Pacific Ocean, Ph.D. thesis, Scripps Inst. of Oceanogr., Univ. of Calif., San Diego, 1996.

Oberhuber, J., An atlas based on the COADS data set: The budgets of heat, buoyancy, and turbulent kinetic energy at the surface of the global ocean, *Rep. 15*, Max-Plank-Inst. für Meteorol., Hamburg, Germany, 1988.

Peters, H., M. Gregg, and T. Sanford, On the parameterization of equatorial turbulence: Effect of fine-scale variations below the range of the diurnal cycle, *J. Geophys. Res.*, *100*, 18,333–18,348, 1995.

Picaut, J., and R. Tournier, Monitoring the 1979–1985 equatorial Pacific current transports with expendable bathythermograph data, *J. Geophys. Res.*, *96*, 3263–3277, 1991.

Qiao, L., and R. Weisberg, The zonal momentum balance of the equatorial undercurrent in the central Pacific, *J. Phys. Oceanogr.*, *27*, 1094–1119, 1997.

Reid, J., On the total geostrophic circulation of the South Pacific Ocean: Flow patterns, tracers, and transports, *Prog. Oceanogr.*, *16*, 1–61, 1986.

Reid, J., and A. Mantyla, On the mid-depth circulation of the North Pacific Ocean, *J. Phys. Oceanogr.*, *8*, 946–951, 1978.

Ridgeway, K., and S. Godfrey, Mass and heat budgets in the East Australian Current: A direct approach, *J. Geophys. Res.*, *99*, 3231–3248, 1994.

Rienecker, M., R. Atlas, S. Schubert, and C. Willett, A comparison of surface wind products over the North Pacific Ocean, *J. Geophys. Res.*, *101*, 1011–1023, 1996.

Roemmich, D., and T. McCallister, Large scale circulation of the North Pacific Ocean, *Prog. Oceanogr.*, *22*, 171–204, 1989.

Spencer, R. W., Global oceanic precipitation from MSU during 1979–91 and comparisons to other climatologies, *J. Clim.*, *6*, 1301–1325, 1993.

Sprintall, J., A. Althaus, D. Roemmich, L. Lehmann, B. Cornuelle, and R. Bailey, High resolution XBT sections in the Pacific and Indian Oceans, 1991–1995, *UCSD/SIO* Ref. 96–28, Scripps Inst. of Oceanogr., La Jolla, Calif., 1996.

Talley, L., Meridional heat transport in the Pacific Ocean, *J. Phys. Oceanogr.*, *14*, 230–241, 1984.

Toole, J., E. Zou, and R. Millard, On the circulation of the upper waters in the western equatorial Pacific Ocean, *Deep Sea Res., Part A*, *35*, 1451–1482, 1988.

Tsuchiya, M., Flow path of the Antarctic Intermediate Water in the western equatorial South Pacific Ocean, *Deep Sea Res., Part A*, *38*, 273–279, 1991.

Weare, B., Uncertainties in estimates of surface heat fluxes derived from marine reports over the tropical and subtropical oceans, *Tellus, Ser. A*, *41*, 357–370, 1989.

Weare, B., P. Strub, and M. Samuel, Annual mean surface heat fluxes in the tropical Pacific Ocean, *J. Phys. Oceanogr.*, *11*, 705–717, 1981.

Webster, P., and R. Lukas, TOGA COARE: The Coupled Ocean-Atmosphere Response Experiment, *Bull. Am. Meteorol. Soc.*, *73*, 1377–1416, 1992.

Weisberg, R., and S. Hayes, Upper ocean variability on the equator in the Pacific at 170°W, *J. Geophys. Res.*, *100*, 20,485–20,498, 1995.

Weisberg, R., and C. Wang, Slow variability in the equatorial west-central Pacific in relation to ENSO, *J. Clim.*, *10*, 1998–2017, 1997.

Weller, R., and S. Anderson, Surface meteorology and air-sea fluxes in the western equatorial Pacific warm pool during the TOGA Coupled

Ocean-Atmosphere Response Experiment, *J. Clim.*, *9*, 1959–1990, 1996.

White, W., Design of a global observing system for gyre-scale upper ocean temperature variability, *Prog. Oceanogr.*, *36*, 169–217, 1995.

Wijffels, S., Exchanges between hemispheres and gyres: A direct approach to the mean circulation of the equatorial Pacific, Ph.D. thesis, Woods Hole Oceanogr. Inst., Woods Hole, Mass., 1993.

Wyrtki, K., and B. Kilonsky, Mean water and current structure during the Hawaii-to-Tahiti Shuttle Experiment, *J. Phys. Oceanogr.*, *14*, 242–254, 1984.

G. Meyers, Marine Laboratory, Division of Oceanography, CSIRO, GPO Box 1538, Hobart, Tasmania 7001, Australia. (e-mail: Gary.Meyers@ml.csiro.au)

M. Morris, Woods Hole Oceanographic Institution, MS 29, Woods Hole, MA 02543. (e-mail: mym@bucky.whoi.edu)

D. Roemmich, Scripps Institution of Oceanography, University of California, San Diego, 9500 Gilman Drive, La Jolla, CA 92093-0230. (e-mail: droemmich@ucsd.edu)

R. Weisberg, Department of Marine Sciences, University of South Florida, 140 Seventh Avenue South, Saint Petersburg, FL 33701. (e-mail: weisberg@ocg6.marine.usf.edu)

(Received May 5, 1997; revised January 8, 1998;
accepted January 16, 1998.)